

# An Energy Management System with Short-Term Fluctuation Reserves and Battery Degradation for Isolated Microgrids

Samuel Córdova, *Student Member, IEEE*, Claudio Cañizares, *Fellow, IEEE*, Álvaro Lorca, *Member, IEEE*, and Daniel E. Olivares, *Member, IEEE*

**Abstract**—Due to the low-inertia and significant renewable generation variability in isolated microgrids, short time-scale fluctuations in the order of seconds can have a large impact on a microgrid’s frequency regulation performance. In this context, the present paper presents a mathematical model for an Energy Management System (EMS) that takes into account the operational impact of the short-term fluctuations stemming from renewable generation rapid changes, and the role that renewable curtailment and batteries, including their degradation, can play to counter-balance these variations. Computational experiments on the real Kasabonika Lake First Nation microgrid and CIGRE benchmark test system show the operational benefits of the proposed EMS, highlighting the need to properly model short-term fluctuations and battery degradation in EMS for isolated microgrids with significant renewable integration.

**Index Terms**—Energy management system, short-term fluctuations, battery degradation, frequency regulation, microgrid operation.

## NOMENCLATURE

### Indices and Sets

$b \in \mathcal{B}$	Battery
$h \in \mathcal{H}$	Dispatch (or long) time interval, $\mathcal{H} = \{1, \dots, H\}$
$i \in \mathcal{I}$	Thermal generator
$j \in \mathcal{J}$	Short time interval, $\mathcal{J} = \{1, \dots, J\}$
$l \in \mathcal{L}$	Partition for piecewise linear battery degradation model

### Parameters

$\mathbf{1}$	Vector of ones of dimension $J$
$C_i^g$	Variable generation costs for generator $i$
$C_i^{ls}$	Load shedding costs
$C_i^{nl}$	No-load costs for generator $i$
$C_i^{su}, C_i^{sd}$	Start-up and shut-down costs for generator $i$

This work was supported by ANID/FONDECYT/1181517, SERC-Chile (ANID/FONDAP/15110019), the Complex Engineering Systems Institute (ANID/FB0816), and NSERC Canada.

S. Córdova and C. Cañizares are with the Department of Electrical and Computer Engineering, University of Waterloo, Waterloo, ON N2L 3G1, Canada (e-mail: scordova@uwaterloo.ca; ccanizares@uwaterloo.ca).

Álvaro Lorca is with the Department of Electrical Engineering, the Department of Industrial and Systems Engineering, and the UC Energy Research Center at Pontificia Universidad Católica de Chile, Santiago, Chile (e-mail: alvarolorca@uc.cl).

Daniel Olivares is with the Faculty of Engineering and Sciences, Universidad Adolfo Ibáñez, and the Complex Engineering Systems Institute, Santiago, Chile (e-mail: daniel.olivares@uai.cl).

$\hat{D}_h$	Average demand forecast during dispatch time interval $h$
$E_b$	Energy capacity limit of battery $b$
$M_i^{up}, M_i^{dn}$	Minimum-up and minimum-down times of generator $i$
$N^w, N^s$	Wind and solar total installed capacities
$\bar{P}_i^g, \underline{P}_i^g$	Maximum and minimum power capacity of generator $i$
$\hat{P}_h^w, \hat{P}_h^s$	Normalized average power forecasts resulting from 1kW wind and solar plants
$\bar{P}_b^\beta$	Maximum power capacity of battery $b$
$S_{b,l}^0$	Initial battery State-of-Charge
$\bar{s}_{b,l}$	State-of-Charge depth range of battery’s $b$ partition $l$
$\Delta T_h$	Time step of dispatch time interval $h$
$\Delta \tau$	Time step of short time intervals $j \in \mathcal{J}$
$\epsilon_\chi, \epsilon_r$	Forecast error and regulation reserve scaling parameters
$\eta_b^c, \eta_b^d$	Charging and discharging efficiency of battery $b$
$\kappa_i^g, \kappa_b^\beta$	Frequency-droop of generator $i$ and battery $b$
$\phi_{b,l}$	Piecewise linear battery degradation coefficient
$\varphi_h^\chi, \varphi_h^r$	Expected reserve utilization of forecast error and regulation reserves

### Variables

$c_{b,l,h}, d_{b,l,h}$	Battery charging and discharging
$ls_h$	Load shedding set-point for dispatch time interval $h$
$n_h^w, n_h^s$	Wind and solar deployed capacities
$\hat{P}_{i,h}^g, \hat{P}_{b,h}^\beta$	Generator and battery average power set-points for dispatch time interval $h$
$P_{i,h}^g, P_{i,h}^\beta$	Reference instantaneous powers provided to generator $i$ and battery $b$
$P'_{i,h}^g, P'_{i,h}^\beta$	Effectively delivered instantaneous powers of generator $i$ and battery $b$
$\hat{P}_h^w, \hat{P}_h^s$	Average wind and solar power forecasts during dispatch time interval $h$
$r_h$	Vector of intra-dispatch fluctuations
$r_h^{mg}$	Microgrid’s regulation signal
$s_{b,l,h}$	Battery State-of-Charge
$u_{i,h}$	ON/OFF status of generator $i$ (binary)
$v_{i,h}, w_{i,h}$	Start-up and shut-down of generator $i$ (binary)

$\alpha_{i,h}^{g,\chi,\uparrow/\downarrow}$	Upward/downward forecast error participation factor of generator $i$
$\alpha_{i,h}^{g,r,\uparrow/\downarrow}$	Upward/downward regulation participation factor of generator $i$
$\alpha_{b,h}^{\beta,\chi,\uparrow/\downarrow}$	Upward/downward forecast error participation factor of battery $b$
$\alpha_{b,h}^{\beta,r,\uparrow/\downarrow}$	Upward/downward regulation participation factor of battery $b$
$\Delta e_{i,h}$	Change in the expected average power of generator $i$ due to reserve provision
$\Delta p_{i,h}^{g,\chi,\uparrow/\downarrow}$	Upward/downward forecast error reserve provided by generator $i$
$\Delta p_{b,l,h}^{\beta,\chi,\uparrow/\downarrow}$	Upward/downward forecast error reserve provided by battery's $b$ partition $l$
$\Delta p_{i,h}^{g,r,\uparrow/\downarrow}$	Upward/downward regulation reserve provided by generator $i$
$\Delta p_{b,l,h}^{\beta,r,\uparrow/\downarrow}$	Upward/downward regulation reserve provided by battery's $b$ partition $l$
$\Delta s_{b,l,h}$	Change in the expected State-of-Charge of battery's $b$ partition $l$ due to reserve provision
$\Delta \phi_{b,l,h}$	Increase in expected battery degradation due to reserve provision
$\zeta_h^{\chi}, \zeta_h^r$	Forecast error and regulation reserve requirements
$\xi$	Uncertainty
$\Phi_{b,l,h}$	Expected resulting battery degradation
$\chi_h$	Average power forecast error during dispatch time interval $h$
$\chi_h^{mg}$	Microgrid's net load forecast error

## I. INTRODUCTION

**M**OTIVATED by the search of cleaner and more efficient generation sources, microgrids are now being studied and deployed due to their potential to facilitate a reliable and efficient integration of Distributed Energy Resources (DER). In this context, several research efforts are presently being made in the design of Energy Management Systems (EMS) for isolated microgrids to enable their economic and reliable operation, resulting in sophisticated EMS models that incorporate features such as phase imbalance, network representations, power sharing, demand response, thermal energy resources, voltage stability, and AC/DC connections [1]–[13].

Unlike conventional power systems, isolated microgrids have low inertia and, more commonly nowadays, significant renewable energy penetration, making them particularly susceptible to poor regulation performance due to generation-load imbalances [14]. This makes it necessary to consider short-term fluctuations (in the scale of seconds) commonly neglected in EMS models. Typically, such models assume a constant, albeit uncertain, renewable generation and demand within dispatch time intervals of 5 min to 1 h, neglecting intra-dispatch fluctuations at lower time scales (e.g., [4]–[13], [15]–[18]). While this simplifies the computational burden thanks to the reduced number of time intervals in the mathematical model, it also results on a sub-estimation of the regulation services required to counterbalance short-term power imbalances stemming from the fast fluctuations, potentially leading

to insufficient reserve allocation and thus degraded regulation performance. This issue is especially relevant for isolated microgrids, since significant variations in renewable generation can be observed in the time frame of seconds [19], which can significantly affect the microgrid's frequency regulation performance due to its low inertia [20].

Previous works on the operational impact of renewable generation short-term fluctuations can be found in the bulk power systems context, with the majority of these focusing on operational security assessments rather than optimal dispatch models (e.g., [21]–[26]). While such works provide relevant reliability insights based on extensive simulations, they do not address the issue of embedding intra-dispatch fluctuations in an optimal dispatch model, especially in the context of microgrids, which is the aim of the current paper. Within the microgrid context, two-layer EMS models have been proposed for the management of fast power fluctuations (e.g., [27], [28]). These types of EMS models feature an open-loop structure and are characterized by two decision-making levels, namely: (i) an upper-level, in charge of determining the optimal dispatch of DER units, and (ii) a lower-level, which uses the dispatch set-points as references and smooths out fast power fluctuations. However, this approach suffers the drawback that dispatch set-points are still determined independently from the short-term power fluctuations, i.e., in open-loop, providing no guarantees of feasibility of the lower-level in the presence of large and fast power fluctuations.

The explicit modeling of intra-dispatch fluctuations in optimal dispatch models, i.e., beyond static reserve needs, is relatively new, with [29]–[31] being the main works that have directly studied this aspect. In general, these works integrate short-term fluctuations by defining: (i) a master problem with a low time resolution that determines units' set-points, and (ii) a sub-problem with a more detailed time resolution that checks if enough slack capacity is left in the units to handle intra-dispatch fluctuations. Thus, feasible dispatch set-points are determined by iteratively solving master and sub-problems through a constraint generation method. Although this approach has proven to be successful in handling fluctuations in the order of 0.5–15 min, significant drawbacks can be identified in these models that prevent their application in modern EMS for isolated microgrids, which require the capability to manage second-to-second fluctuations. Specifically, the dependency of the sub-problem's number of variables on the time resolution used for modeling intra-dispatch fluctuations leads to the number of decision variables rapidly increasing as the time resolution approaches a second-to-second time scale, potentially resulting in a computationally intractable model. Another issue is the fact that in the presented simulations, simplified synthetic short-term power fluctuations are used to assess the performance of the proposed models, raising the question of whether the tested power variations are realistic, and, consequently, if the presented analyses and results can be applied in practice.

An additional relevant aspect to consider in EMS design is which flexibility strategies are considered for the management of power variations. Within such strategies, the use of battery and renewable curtailment are of particular interest, as

batteries can provide energy shifting and frequency regulation services [32], and renewable curtailment can provide balancing and regulation services [20], [33]. Accordingly, most modern EMS models for isolated microgrids already incorporate the capability of both aforementioned flexibility strategies for managing fluctuations across dispatch time-intervals in the range of 5 min to 1h [4]–[13]. However, none of these works consider the capability of batteries and renewable curtailment to handle second-to-second intra-dispatch fluctuations.

Another important related topic to consider for EMS design is the battery degradation resulting from their repeated charging/discharging, which has commonly been neglected in existing microgrid EMS models under the assumption that degradation costs are relatively low on an operational scale (e.g., [4]–[11]). However, various recent papers show that battery operation can significantly impact the battery's life (e.g., [34]), making degradation a relevant factor in operations. Thus, more recent works embed battery degradation within EMS models; however, most of them either employ a fixed discharging-charging cost and thus sacrifice degradation model accuracy [12], [13], [29], [35], or use accurate but computationally expensive representations based on auxiliary binary variables [28], [36]. Other works propose degradation models that effectively balance degradation model accuracy and computational tractability such as [37] and [38], but in the context of bulk power systems, which significantly differ from microgrids.

Based on the discussion above, the present paper develops a computationally tractable centralized EMS that incorporates intra-dispatch fluctuations and their impact on microgrid operation, while considering the flexibility that both batteries and renewable curtailment can provide. Moreover, the proposed EMS incorporates the effect of battery degradation stemming from the provision of energy shifting and regulation services, while balancing computational performance and degradation modeling accuracy. Since directly adding more time intervals to model fluctuations in the time frame of seconds would yield a computationally intractable formulation, intra-dispatch fluctuations are characterized here through a set of low-dimension statistical metrics, allowing to mathematically describe the operational impact of such fast fluctuations in a computationally efficient way. Thus, the contributions of this paper can be summarized as follows:

- 1) Precise and computationally efficient models to describe intra-dispatch fluctuations and battery degradation are developed, which serve as the basis for the design of an efficient and practical EMS model.
- 2) Novel mathematical models to describe the impacts and constraints associated with the provision of regulation services are presented, namely, system reserve needs and utilization, battery degradation, renewable curtailment, and limitations imposed by the frequency control mechanism.
- 3) Computational experiments on two realistic test systems are presented to demonstrate that modeling intra-dispatch fluctuations and battery degradation through the proposed EMS enables the reduction of total operating costs, battery degradation, and thermal-unit cycling. The

experiments show as well that modeling rapid power fluctuations allows to quantify the economic benefits of including a supplementary control instead of using a simpler droop-only control. All simulations are performed using actual field measurements of renewable generation and demand, ensuring the validity of the analyses and results.

The rest of the paper is organized as follows: Section II presents the mathematical models used for intra-dispatch fluctuations and battery degradation. Section III then discusses reserves and their modeling. Using the models of both previous sections, the proposed EMS model is formulated in Section IV. Computational experiments and their results are discussed in Section V. Finally, the main conclusions of the paper and future work are discussed in Section VI.

## II. INTRA-DISPATCH FLUCTUATIONS AND BATTERY DEGRADATION MODELS

In this section, novel computationally efficient models to describe intra-dispatch fluctuations and battery degradation are developed. These models serve as the basis for deriving the mathematical expressions that describe the computationally tractable EMS model proposed in this paper.

### A. Intra-Dispatch Fluctuations Model

One of the main challenges of modeling intra-dispatch fluctuations in EMS is computational tractability. As time variability of renewable generation and demand is usually captured in EMS models by defining different time intervals, directly using a detailed time-resolution in the order of seconds would result on a dramatic increase in the number of decision variables, yielding a computational intractable model. Hence, a computationally efficient representation of intra-dispatch fluctuations is developed in this paper, which is discussed in detail here, and is based on considering two different time frames: one for dispatch (or long) time intervals  $h \in \mathcal{H} = \{1, \dots, H\}$ , and another for short time intervals  $j \in \mathcal{J} = \{1, \dots, J\}$ . This allows splitting the generic instantaneous power vector  $\mathbf{p}_h$  during dispatch time interval  $h$  into long and short term components as follows:

$$\mathbf{p}_h = \underbrace{[\hat{p}_h + \chi_h(\xi)]}_{\text{long term}} \mathbf{1} + \underbrace{\mathbf{r}_h(\xi)}_{\text{short term}} \quad (1)$$

where  $\mathbf{p}_h = [p_{h,1}, \dots, p_{h,j}, \dots, p_{h,J}]$ ;  $\mathbf{1}$  is a vector of ones of dimension  $J$ ;  $\hat{p}_h$  is the average power forecast; and  $\chi_h$  is the average power forecast error, which is affected by uncertainty  $\xi$ . Thus, intra-dispatch fluctuations are described by vector  $\mathbf{r}_h = [r_{h,1}, \dots, r_{h,j}, \dots, r_{h,J}]$ , which is also affected by uncertainty. Note that  $\hat{p}_h$  and  $\chi_h$  are constant during the dispatch time interval  $h$ , and thus have a time resolution of  $\Delta T_h$ . In contrast,  $\mathbf{r}_h$  depends also on the short time interval  $j$ , and thus has a time step of length  $\Delta\tau \ll \Delta T_h$ . Fig. 1 depicts an example in which measurements for the Kasabonika Lake First Nation (KLFN) microgrid [39], with a resolution of  $\Delta\tau = 1\text{s}$ , are used to build: (i) average powers  $\hat{p}_h$ , which are constant during dispatch time intervals of length

$\Delta T_h = 5\text{min} \forall h \in \mathcal{H}$ ; and (ii) intra-dispatch fluctuations  $\mathbf{r}_h$ , that oscillate around the average powers. In this example, forecast errors are not present, i.e.,  $\chi_h = 0 \forall h \in \mathcal{H}$ .

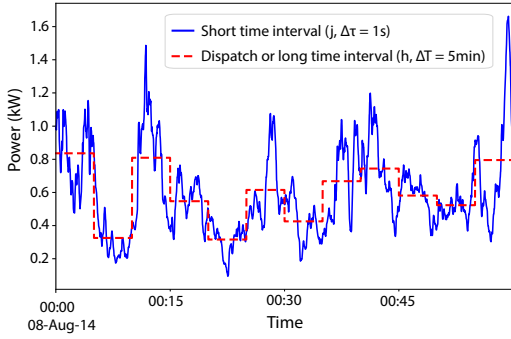


Fig. 1. Average powers and intra-dispatch fluctuations for a 10 kW wind plant at the KLFN microgrid [39].

Formulation (1) allows the formal definition of a novel computationally efficient representation of the vector of intra-dispatch fluctuations  $\mathbf{r}_h$ , referred to as *feature-based representation* in this paper. The key idea is that instead of directly using the high-dimensional vector  $\mathbf{r}_h$  in the EMS model (as in [29]–[31]), only the most relevant features of such vector are considered, avoiding the need to define decision variables for each short time interval  $j \in \mathcal{J}$ , thus significantly reducing computational burden. In this paper, the standard deviation (std) and mean absolute deviation (mad) statistical metrics are selected as the features that characterize  $\mathbf{r}_h$ , since these can be linked to reserve sizing and reserve utilization, as described later in Sections III-B and IV-A. Thus, the feature-based representation of  $\mathbf{r}_h$  is as follows:

$$\mathbf{v}_h = \begin{bmatrix} \text{std}(\mathbf{r}_h) \\ \text{mad}(\mathbf{r}_h) \end{bmatrix} \quad (2)$$

where  $\mathbf{v}_h$  is a vector of dimension equal to 2, which is significantly lower than  $J = \dim(\mathbf{r}_h)$ . Note that this idea can easily be extended to incorporate other relevant features.

### B. Battery Degradation Model

The lifetime of batteries depends on a number of external stress factors that degrade its components, such as cycle Depth-of-Discharge (DoD), cell temperature, average State-of-Charge (SoC), and calendar time. Given that the emphasis of this paper is on operations, the modeling here focuses on the degradation caused by the repeated charging and discharging of the battery, commonly referred to as cycle aging [34]. In particular, a piecewise degradation model based on [37] is used, as it offers a good balance between model accuracy and computational performance, as explained next.

In general, the degradation caused by cycle aging can be described as follows [34]:

$$f^{cyc}(\boldsymbol{\rho}, \boldsymbol{\theta}) = \sum_{k=1}^K \rho_k \Gamma_{\theta}(\theta_k), \quad [\boldsymbol{\rho}, \boldsymbol{\theta}]^T = \mathbf{f}^{id}(\mathbf{s}) \quad (3)$$

where  $f^{cyc}(\cdot) \in [0, 1]$  represents the cycle aging,  $\Gamma_{\theta}(\cdot)$  is the DoD stress factor model for battery degradation, and  $K$  is the

total number of cycles. Each cycle  $k$  is characterized by its DoD  $\theta_k$ , and count  $\rho_k$ , which can take the value of either 1 (full-cycle) or 0.5 (half-cycle). The values of  $\rho_k$ ,  $\theta_k$ , and  $K$  are determined through the cycle identification algorithm  $\mathbf{f}^{id}(\cdot)$ , which is a function of the battery's SoC profile  $\mathbf{s}$ , and in this paper corresponds to the rainflow cycle counting algorithm, as in [34], [37], [38]. An illustrative example of the application of the rainflow cycle counting algorithm for a given SoC profile is shown in Fig. 2. The output of the cycle identification algorithm yields a total of  $K = 5$  cycles, with  $k = \{1, 2, 4, 5\}$  being half-cycles, and  $k = 3$  being the only full-cycle.

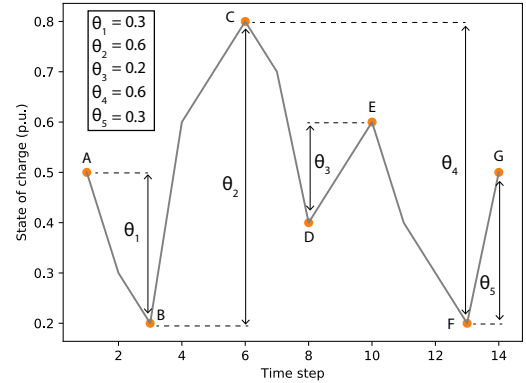


Fig. 2. Example of the application of the rainflow cycle counting algorithm for a given SoC profile

Equation (3) cannot be directly incorporated in an optimization model, since  $\mathbf{f}^{id}(\cdot)$  is non-analytic, and  $\Gamma_{\theta}(\cdot)$  is convex but non-linear in practical settings [34]. To circumvent this, a piecewise linear representation based on [37] is formulated, for which the battery's cycle depth range is split into even partitions  $l \in \mathcal{L}$ . Assuming that only half-cycles are identified, the degradation of battery  $b \in \mathcal{B}$  can be described as follows:

$$f_b^{cyc}(\mathbf{c}, \mathbf{d}) = \frac{\hat{\phi}_{b,l}}{2} \frac{\Delta t}{E_b} \sum_{t \in \mathcal{T}} \sum_{l \in \mathcal{L}} \left( \eta_b^c c_{b,l,t} + \frac{d_{b,l,t}}{\eta_b^d} \right) \quad (4a)$$

$$s_{b,l,t} - s_{b,l,t-1} = \frac{\Delta t}{E_b} \left( \eta_b^c c_{b,l,t} - \frac{d_{b,l,t}}{\eta_b^d} \right) \quad (4b)$$

$$0 \leq s_{b,l,t} \leq \bar{s}_{b,l} \quad \forall b \in \mathcal{B}, l \in \mathcal{L}, t \in \mathcal{T} \quad (4c)$$

where  $\mathcal{T}$  is a set of generic time intervals  $t$  with time-step length  $\Delta t$ ;  $c_{b,l,t}$  is the charging and  $d_{b,l,t}$  the discharging of battery's  $b$  partition  $l$  at time  $t$ ;  $E_b$ ,  $\eta_b^c$ , and  $\eta_b^d$  are the battery's energy capacity, charging efficiency, and discharging efficiency, respectively; and  $\hat{\phi}_{b,l}$  is the piecewise linear degradation coefficient. Note that each battery's  $b$  partition  $l$  has its own SoC  $s_{b,l,t}$ , which is bounded by the partition's depth range  $\bar{s}_{b,l}$ .

It is worth highlighting that the piecewise linear degradation model (4) focuses on the cycle DoD as the main driver of battery degradation, neglecting other factors such as ambient temperature and average SoC. These other factors are omitted due to their small impact relative to cycle DoD when proper external controllers are in place (e.g., cell temperature control and SoC constraints), as per [37].

### III. RESERVES AND REGULATION MODELING

Following the characterization of instantaneous power vectors in (1), this section discusses the definition of reserves to handle forecast errors and intra-dispatch fluctuations. Specifically, methods for reserve sizing and allocation are developed, and tools for assessing the security provided by such reserves are presented.

#### A. Forecast Error Reserve

Most EMS models consider reserves to handle forecast errors, which are typically modeled as a percentage of the expected renewable generation and demand (see e.g., [4]–[9]). This same principle is used here to determine the forecast error reserve needs. From (1), one can describe the microgrid's net load forecast error as follows:

$$\chi_h^{mg}(\xi) = \hat{D}_h \tilde{\chi}_h^d(\xi) - \hat{p}_h^w \tilde{\chi}_h^w(\xi) - \hat{p}_h^s \tilde{\chi}_h^s(\xi) \quad (5)$$

where  $\hat{D}_h$ ,  $\hat{p}_h^w$ , and  $\hat{p}_h^s$  are the forecast average powers during dispatch time interval  $h$  corresponding to demand, wind generation, and solar generation, respectively. Errors associated with each forecast are described by the normalized zero-mean random scalars  $\tilde{\chi}_h^d$ ,  $\tilde{\chi}_h^w$ , and  $\tilde{\chi}_h^s$ .

Based on (5), and assuming statistical independence, the standard deviation of the microgrid's net load can be computed as follows:

$$\text{std}(\chi_h^{mg}) = \left[ \left( \hat{D}_h \tilde{\sigma}_h^{\chi,d} \right)^2 + \left( \hat{p}_h^w \tilde{\sigma}_h^{\chi,w} \right)^2 + \left( \hat{p}_h^s \tilde{\sigma}_h^{\chi,s} \right)^2 \right]^{1/2} \quad (6)$$

where  $\tilde{\sigma}_h^{\chi,d} = \text{std}(\tilde{\chi}_h^d)$ ,  $\tilde{\sigma}_h^{\chi,w} = \text{std}(\tilde{\chi}_h^w)$ , and  $\tilde{\sigma}_h^{\chi,s} = \text{std}(\tilde{\chi}_h^s)$  can be estimated from normalized historical samples of forecast errors  $\chi_h^d/\hat{D}_h$ ,  $\chi_h^w/\hat{p}_h^w$ , and  $\chi_h^s/\hat{p}_h^s$ , respectively. Thus, the forecast error reserve requirement is given by:

$$\zeta_h^\chi = \epsilon_\chi \text{std}(\chi_h^{mg}) \quad (7)$$

where the confidence level can be adjusted through the parameter  $\epsilon_\chi$ .

#### B. Regulation Reserve

Typical EMS models do not explicitly represent intra-dispatch fluctuations, nor explicitly consider these when computing total reserve requirements (see e.g., [4]–[13]). However, as discussed in Section I, properly accounting for short-term fluctuations is important in isolated microgrids with low inertia and significant renewable integration. Thus, unlike previous EMS models, an especially-dedicated regulation reserve is considered here, which aims to handle the regulation signal stemming from fast fluctuations of demand and renewable generation. From (1), such regulation signal can be defined as follows:

$$\mathbf{r}_h^{mg}(\xi) = \hat{D}_h \tilde{\mathbf{r}}_h^d(\xi) - \hat{p}_h^w \tilde{\mathbf{r}}_h^w(\xi) - \hat{p}_h^s \tilde{\mathbf{r}}_h^s(\xi) \quad (8)$$

where  $\tilde{\mathbf{r}}_h^d$ ,  $\tilde{\mathbf{r}}_h^w$ , and  $\tilde{\mathbf{r}}_h^s$  are zero-mean random vectors representing the normalized intra-dispatch fluctuations stemming from demand, wind generation, and solar generation, respectively.

Based on (8), and following a similar procedure as in Section III-A, the standard deviation of the regulation signal can be computed as:

$$\text{std}(\mathbf{r}_h^{mg}) = \left[ \left( \hat{D}_h \tilde{\sigma}_h^{\mathbf{r},d} \right)^2 + \left( \hat{p}_h^w \tilde{\sigma}_h^{\mathbf{r},w} \right)^2 + \left( \hat{p}_h^s \tilde{\sigma}_h^{\mathbf{r},s} \right)^2 \right]^{1/2} \quad (9)$$

where  $\tilde{\sigma}_h^{\mathbf{r},d} = \text{std}(\tilde{\mathbf{r}}_h^d)$ ,  $\tilde{\sigma}_h^{\mathbf{r},w} = \text{std}(\tilde{\mathbf{r}}_h^w)$ , and  $\tilde{\sigma}_h^{\mathbf{r},s} = \text{std}(\tilde{\mathbf{r}}_h^s)$ . However, note that in this case, standard deviations are computed by concatenating normalized historical samples of  $r_{j,h}^d/\hat{D}_h$ ,  $r_{j,h}^w/\hat{p}_h^w$ , and  $r_{j,h}^s/\hat{p}_h^s$ , since  $\tilde{\mathbf{r}}$  is a random vector of dimension  $J$ . Furthermore, notice that standard deviations only depend on dispatch time interval  $h \in \mathcal{H}$ , as the short time interval index  $j \in \mathcal{J}$  is avoided in accordance with the feature-based approach (2).

From (9), the regulation reserve requirement can directly be defined, as follows:

$$\zeta_h^{\mathbf{r}} = \epsilon_{\mathbf{r}} \text{std}(\mathbf{r}_h^{mg}) \quad (10)$$

where the confidence level can be adjusted through the parameter  $\epsilon_{\mathbf{r}}$ .

#### C. Reserve Allocation

The reserves previously defined in Sections III-A and III-B require the definition of their corresponding upward and downward reserve constraints to ensure enough capacity margins are kept. Assuming that reserves can be provided by thermal generators  $i \in \mathcal{I}$  and batteries  $b \in \mathcal{B}$ , the following forecast error  $\chi$  reserve constraints can be obtained:

$$\sum_{i \in \mathcal{I}} \Delta p_{i,h}^{g,\chi,\uparrow/\downarrow} + \sum_{b \in \mathcal{B}} \sum_{l \in \mathcal{L}} \Delta p_{b,l,h}^{\beta,\chi,\uparrow/\downarrow} = \zeta_h^\chi \quad \forall h \in \mathcal{H} \quad (11)$$

where  $\Delta p_{i,h}^{g,\chi,\uparrow/\downarrow}$  is the upward ( $\uparrow$ )/downward ( $\downarrow$ ) forecast error reserve provided by generator  $i$ , and  $\Delta p_{b,l,h}^{\beta,\chi,\uparrow/\downarrow}$  is the upward/downward forecast error reserve provided by battery's  $b$  partition  $l$ . The regulation  $\mathbf{r}$  reserve constraints can be defined similarly as follows:

$$\sum_{i \in \mathcal{I}} \Delta p_{i,h}^{g,\mathbf{r},\uparrow/\downarrow} + \sum_{b \in \mathcal{B}} \sum_{l \in \mathcal{L}} \Delta p_{b,l,h}^{\beta,\mathbf{r},\uparrow/\downarrow} = \zeta_h^{\mathbf{r}} \quad \forall h \in \mathcal{H} \quad (12)$$

where  $\Delta p_{i,h}^{g,\mathbf{r},\uparrow/\downarrow}$  is the upward/downward regulation reserve provided by generator  $i$ , and  $\Delta p_{b,l,h}^{\beta,\mathbf{r},\uparrow/\downarrow}$  is the upward/downward regulation reserve provided by battery's  $b$  partition  $l$ .

The reserve allocation defined by variables  $\Delta p$  indicate how the mismatches caused by forecast errors and intra-dispatch fluctuations are shared among generators and batteries. Specifically, power sharing is dictated by the participation factors  $\alpha$ , defined as follows:

$$\alpha_{i,h}^{g,\chi,\uparrow/\downarrow} = \Delta p_{i,h}^{g,\chi,\uparrow/\downarrow} / \zeta_h^\chi \quad (13a)$$

$$\alpha_{i,h}^{g,\mathbf{r},\uparrow/\downarrow} = \Delta p_{i,h}^{g,\mathbf{r},\uparrow/\downarrow} / \zeta_h^{\mathbf{r}} \quad (13b)$$

$$\alpha_{b,h}^{\beta,\chi,\uparrow/\downarrow} = \sum_{l \in \mathcal{L}} \Delta p_{b,l,h}^{\beta,\chi,\uparrow/\downarrow} / \zeta_h^\chi \quad (13c)$$

$$\alpha_{b,h}^{\beta,\mathbf{r},\uparrow/\downarrow} = \sum_{l \in \mathcal{L}} \Delta p_{b,l,h}^{\beta,\mathbf{r},\uparrow/\downarrow} / \zeta_h^{\mathbf{r}} \quad (13d)$$

Thus, the participation factors are determined by the share of the total reserve that is provided by each generator and battery, analogous to the participation factors in an Automatic Generation Control (AGC) scheme [40]. From (1) and (13), the reference instantaneous power provided to generator  $i$  can then be defined as:

$$\begin{aligned} p_{i,h}^g = & \left[ \hat{p}_{i,h}^g + \alpha_{i,h}^{g,\chi,\uparrow} \chi_h^{mg+}(\xi) - \alpha_{i,h}^{g,\chi,\downarrow} \chi_h^{mg-}(\xi) \right] \mathbf{1} \\ & + \alpha_{i,h}^{g,r,\uparrow} r_h^{mg+}(\xi) - \alpha_{i,h}^{g,r,\downarrow} r_h^{mg-}(\xi) \end{aligned} \quad (14)$$

where  $\hat{p}_{i,h}^g$  denotes the generation set-point or average power of generator  $i$  during dispatch time interval  $h$ ; and positive and negative parts are described  $\chi_h^{mg+} = \max\{\chi_h^{mg}, 0\}$ ;  $\chi_h^{mg-} = \max\{-\chi_h^{mg}, 0\}$ , which also applies for  $r^{mg+}$  and  $r^{mg-}$ . Similarly, the reference instantaneous power provided to battery  $b$  can be described by:

$$\begin{aligned} p_{b,h}^\beta = & \left[ \hat{p}_{b,h}^\beta + \alpha_{b,h}^{\beta,\chi,\uparrow} \chi_h^{mg+}(\xi) - \alpha_{b,h}^{\beta,\chi,\downarrow} \chi_h^{mg-}(\xi) \right] \mathbf{1} \\ & + \alpha_{b,h}^{\beta,r,\uparrow} r_h^{mg+}(\xi) - \alpha_{b,h}^{\beta,r,\downarrow} r_h^{mg-}(\xi) \end{aligned} \quad (15)$$

where the battery set-point is given by  $\hat{p}_{b,h}^\beta = \sum_{l \in \mathcal{L}} (d_{b,l,h} - c_{b,l,h})$ . It is important to highlight that (14) and (15) might violate the capacity limits of generators and batteries in the presence of unexpectedly large power fluctuation, as later discussed in Section III-D.

#### D. Reserve Security Assessment

The reference instantaneous powers provided to generators  $p_{i,h}^g$  in (14) and batteries  $p_{b,h}^\beta$  in (15) are computed based on estimated reserve needs, which might not be sufficient in the event of unexpectedly large short-term power variations. As discussed in Section I, this is especially relevant for isolated microgrids, since it would lead to generators and batteries rapidly hitting their capacity limits, affecting the overall system regulation performance. Based on this observation, a differentiation is made between: (i) reference instantaneous powers  $p_{i,h}^g$  and  $p_{b,h}^\beta$ , which might violate power and energy capacity limits, and (ii) effectively delivered instantaneous powers  $p'_{i,h}^g$  and  $p'_{b,h}^\beta$ , which enforce such capacity limits.

The aforementioned definitions allow the design of a security assessment metric to quantify the regulation performance of a particular reserve sizing and allocation method, which is referred here as *limit-hit probability* (LHP), and is defined as follows:

$$\text{LHP} = \mathcal{P} \left[ \left( \exists i : p_{i,h}^g \neq p'_{i,h}^g \right) \cup \left( \exists b : p_{b,h}^\beta \neq p'_{b,h}^\beta \right) \right] \quad (16)$$

This metric measures the frequency (or probability) that the capacity limits of the DER units are reached due to insufficient reserve allocation, leading to differences between reference and delivered instantaneous powers and thus inadequate tracking of the regulation signal.

## IV. ENERGY MANAGEMENT SYSTEM

In this section, the definitions and expressions previously derived in Sections II and III are used to design a computationally tractable EMS model that incorporates intra-dispatch fluctuations and battery degradation.

#### A. Operational Impact of Reserve Provision

Typical EMS models assume that the impact of reserve provision is limited to narrowing the range of feasible average power set-points [4]–[9]. For generators, this can be modeled by the following constraints:

$$\hat{p}_{i,h}^g + \Delta p_{i,h}^{g,\chi,\uparrow} + \Delta p_{i,h}^{g,r,\uparrow} \leq \bar{P}_i^g u_{i,h} \quad \forall i \in \mathcal{I}, h \in \mathcal{H} \quad (17a)$$

$$\hat{p}_{i,h}^g - \Delta p_{i,h}^{g,\chi,\downarrow} - \Delta p_{i,h}^{g,r,\downarrow} \geq \underline{P}_i^g u_{i,h} \quad \forall i \in \mathcal{I}, h \in \mathcal{H} \quad (17b)$$

where  $\bar{P}_i^g$  and  $\underline{P}_i^g$  are generator  $i$ 's maximum and minimum power; and  $u_{i,h}$  is a binary variable indicating the generator's ON/OFF status. Similarly, for batteries, the following constraints apply:

$$\sum_{l \in \mathcal{L}} \left( c_{b,l,h} + \Delta p_{b,l,h}^{\beta,\chi,\downarrow} + \Delta p_{b,l,h}^{\beta,r,\downarrow} \right) \leq \bar{P}_b^\beta \quad \forall b \in \mathcal{B}, h \in \mathcal{H} \quad (18a)$$

$$\sum_{l \in \mathcal{L}} \left( d_{b,l,h} + \Delta p_{b,l,h}^{\beta,\chi,\uparrow} + \Delta p_{b,l,h}^{\beta,r,\uparrow} \right) \leq \bar{P}_b^\beta \quad \forall b \in \mathcal{B}, h \in \mathcal{H} \quad (18b)$$

where  $\bar{P}_b^\beta$  is battery  $b$ 's maximum power capacity. Furthermore, based on (4), constraints to ensure enough energy is saved for battery reserve provision, assuming the worst-case scenario of energy requirement for the following dispatch time interval, can be defined as follows:

$$\begin{aligned} s_{b,l,h-1} + \frac{\Delta T_h \eta_b^c}{E_b} \left( c_{b,l,h} + \Delta p_{b,l,h}^{\beta,\chi,\downarrow} + \Delta p_{b,l,h}^{\beta,r,\downarrow} \right) \\ - \frac{\Delta T_h}{E_b \eta_b^d} d_{b,l,h} \leq \bar{s}_{b,l} \quad \forall b \in \mathcal{B}, l \in \mathcal{L}, h \in \mathcal{H} \end{aligned} \quad (19a)$$

$$\begin{aligned} s_{b,l,h-1} - \frac{\Delta T_h}{E_b \eta_b^d} \left( d_{b,l,h} + \Delta p_{b,l,h}^{\beta,\chi,\uparrow} + \Delta p_{b,l,h}^{\beta,r,\uparrow} \right) \\ + \frac{\Delta T_h \eta_b^c}{E_b} c_{b,l,h} \geq 0 \quad \forall b \in \mathcal{B}, l \in \mathcal{L}, h \in \mathcal{H} \end{aligned} \quad (19b)$$

In addition to the aforementioned constraints, reserves have additional impacts on operation in practice. As discussed in Section III-C, reserves also dictate how real-time mismatches are shared among generators and batteries, and thus have an impact on their instantaneous power outputs. Thus, and unlike previous EMS models, the modeling is here extended to also include this effect, which in turn influences the expected average thermal generation, battery SoC, and battery degradation, as described next.

First, based on the feature-based representation (2), the novel concept of *Expected Reserve Utilization* (ERU) is introduced, which quantifies how much of the allocated reserve is expected to be deployed on average. This metric is especially relevant for forecast error reserves and regulation reserves, which, unlike contingency reserves, are continuously being deployed to handle real-time mismatches. In this paper, the ERU of forecast error and regulation reserves is estimated by computing the ratio between the mean absolute deviation (mad) and total reserve requirements  $\zeta$ , as follows:

$$\varphi_h^\chi = \min \{1, \text{mad}(\chi_h^{mg}) / \zeta_h^\chi\} = \min \{1, \mathcal{G}^\mathcal{K}(\chi_h^{mg}) / \epsilon_\chi\} \quad (20a)$$

$$\varphi_h^r = \min \{1, \text{mad}(r_h^{mg}) / \zeta_h^r\} = \min \{1, \mathcal{G}^\mathcal{K}(r_h^{mg}) / \epsilon_r\} \quad (20b)$$

where  $\mathcal{G}^\mathcal{K}(\cdot) = \text{mad}(\cdot) / \text{std}(\cdot)$  is the Geary's kurtosis [41]. Note, however, that other methods for estimating the ERU can also be used.

For thermal generators, the ERU allows modeling the change in the expected average power of generator  $i$  during dispatch time interval  $h$  due to reserve provision, as follows:

$$\Delta e_{i,h} = \frac{\varphi_h^x}{2} \left( \Delta p_{i,h}^{g,\chi,\uparrow} - \Delta p_{i,h}^{g,\chi,\downarrow} \right) + \varphi_h^r \left( \Delta p_{i,h}^{g,r,\uparrow} - \Delta p_{i,h}^{g,r,\downarrow} \right) \quad (21)$$

Note that  $\varphi_h^x$  is multiplied by 1/2 since either a positive or negative forecast error reserve will be deployed at each dispatch time interval  $h$ . This is not needed for  $\varphi_h^r$ , since both positive and negative regulation reserves will always be deployed at each dispatch time interval  $h$ .

For batteries, ERU can be used to describe the change in the expected SoC of battery's  $b$  partition  $l$  due to reserve provision, as follows:

$$\Delta s_{b,l,h} = \frac{\varphi_h^x}{2} \frac{\Delta T_h}{E_b} \left( \eta_b^c \Delta p_{b,l,h}^{\beta,\chi,\downarrow} - \frac{\Delta p_{b,l,h}^{\beta,\chi,\uparrow}}{\eta_b^d} \right) + \varphi_h^r \frac{\Delta T_h}{E_b} \left( \eta_b^c \Delta p_{b,l,h}^{\beta,r,\downarrow} - \frac{\Delta p_{b,l,h}^{\beta,r,\uparrow}}{\eta_b^d} \right) \quad (22)$$

Thus, the expected SoC at the end of dispatch time interval  $h$ , resulting from both energy shifting and reserve provision can be described as follows:

$$s_{b,l,h} - s_{b,l,h-1} = \frac{\Delta T_h}{E_b} \left( \eta_b^c c_{b,l,h} - \frac{d_{b,l,h}}{\eta_b^d} \right) + \Delta s_{b,l,h} \quad (23a)$$

$$0 \leq s_{b,l,h} \leq \bar{s}_{b,l} \quad \forall b \in \mathcal{B}, l \in \mathcal{L}, h \in \mathcal{H} \quad (23b)$$

The ERU also allows to describe the expected increase in battery degradation due to reserve provision as follows:

$$\Delta \phi_{b,l,h} = \frac{\hat{\phi}_{b,l}}{2} \frac{\varphi_h^x}{2} \frac{\Delta T_h}{E_b} \left( \eta_b^c \Delta p_{b,l,h}^{\beta,\chi,\downarrow} + \frac{\Delta p_{b,l,h}^{\beta,\chi,\uparrow}}{\eta_b^d} \right) + \frac{\hat{\phi}_{b,l}}{2} \varphi_h^r \frac{\Delta T_h}{E_b} \left( \eta_b^c \Delta p_{b,l,h}^{\beta,r,\downarrow} + \frac{\Delta p_{b,l,h}^{\beta,r,\uparrow}}{\eta_b^d} \right) \quad (24)$$

where this equation is based on the piecewise degradation model (4). Thus, the expected total battery degradation resulting from energy shifting and reserve provision is:

$$\Phi_{b,l,h} = \frac{\hat{\phi}_{b,l}}{2} \frac{\Delta T_h}{E_b} \left( \eta_b^c c_{b,l,h} + \frac{d_{b,l,h}}{\eta_b^d} \right) + \Delta \phi_{b,l,h} \quad (25)$$

### B. Renewable Curtailment

Another relevant feature commonly neglected in EMS models is the use of renewable curtailment for short-term fluctuation management [4]–[13]. Since intra-dispatch fluctuations are mainly a byproduct of non-dispatchable renewable generation, renewable curtailment can be used to reduce such fluctuations and thus reserve needs. To model this phenomenon, the high correlation in the resource availability of the microgrid's renewable plants is exploited, which stems from the geographical proximity of the microgrid's units. Thus, wind and solar generation can be lumped into one equivalent renewable plant

for each, yielding the following equations for the total wind and solar forecast average powers  $\hat{p}_h^w$  and  $\hat{p}_h^s$ :

$$\hat{p}_h^w = n_h^w \hat{P}_h^w, \quad \hat{p}_h^s = n_h^s \hat{P}_h^s \quad \forall h \in \mathcal{H} \quad (26)$$

$$n_h^w \leq N^w, \quad n_h^s \leq N^s \quad \forall h \in \mathcal{H} \quad (27)$$

where  $N^w$  and  $N^s$  are the total wind and solar installed capacities in kW;  $\hat{P}_h^w$  and  $\hat{P}_h^s$  are the normalized forecast average powers resulting from 1 kW wind and solar plants; and  $n_h^w$  and  $n_h^s$  are EMS decision variables hereinafter referred as the wind and solar *deployed capacities*. The latter are used to control the amount of renewable curtailment in the microgrid, which is determined based on the percentages  $n_h^w/N^w$  and  $n_h^s/N^s$  of the total available wind and solar generation to be injected into the system.

Equation (26) not only impacts the average power injected by renewable sources, but also the microgrid's net load forecast error  $\chi_h^{mg}$  in (5) and regulation signal  $r_h^{mg}$  in (8). Thus, the forecast error and regulation reserve needs  $\zeta_h^x$  and  $\zeta_h^r$ , originally described by eqs. (5)-(10), are then a function of wind and solar deployed capacities  $(n_h^w, n_h^s)$ , as follows:

$$\zeta_h^{\chi/r} = \epsilon_{\chi/r} \left[ \left( \hat{D}_h \tilde{\sigma}_h^{\chi/r,d} \right)^2 + \left( n_h^w \hat{P}_h^w \tilde{\sigma}_h^{\chi/r,w} \right)^2 + \left( n_h^s \hat{P}_h^s \tilde{\sigma}_h^{\chi/r,s} \right)^2 \right]^{1/2} \quad (28)$$

which captures the capability of using renewable curtailment to reduce the overall system reserve needs. Eq. (28) is non-convex in  $(n_h^w, n_h^s)$ , and thus computationally inefficient. To obtain an efficient convex formulation, the fact that  $\hat{D}_h \sigma_h^{\chi/r,d}$  is large in practical settings is exploited, which allows replacing the non-convex square root function by a linear interpolation between points  $(0, 0)$  and  $(N^w, N^s)$ . Thus, a set of supporting hyperplanes can be used to represent reserve needs  $\zeta_h^x$  and  $\zeta_h^r$ , which can be iteratively updated through a cutting-planes algorithm [42].

It is also important to highlight that due to the dependence of reserve needs  $\zeta_h^x$  and  $\zeta_h^r$  on  $(n_h^w, n_h^s)$ , the ERUs in (20) are also affected by  $(n_h^w, n_h^s)$ . To avoid overcomplicating the model and keep computational tractability, it is assumed that both  $\chi_h^{mg}$  and  $r_h^{mg}$  resemble a normal distribution, and thus  $\mathcal{G}^{\mathcal{K}} = \sqrt{2/\pi} \approx 0.8$  regardless of the values of  $(n_h^w, n_h^s)$ , eliminating the dependence of the ERUs on the deployed capacities.

### C. Frequency Control Mechanism

As discussed in Section II-A, intra-dispatch fluctuations describe short-term oscillations in the order of seconds. Under this time frame, the microgrid's frequency control mechanism might impose limitations on the way power mismatches are shared, making its modeling relevant. Typically, microgrids have a droop control which may or may not be accompanied by a supplementary control for frequency recovery [1], similar to AGC. In the case of a droop-only control, the intra-dispatch fluctuations will be shared among generators and batteries

according to their droop  $\kappa$ , requiring the addition of power sharing constraints  $\forall h \in \mathcal{H}$ , as follows [6]:

$$\frac{\kappa_b^\beta}{\overline{P}_b^\beta} \sum_{l \in \mathcal{L}} \Delta p_{b,l,h}^{\beta,r,\uparrow/\downarrow} = \frac{\kappa_{b'}^\beta}{\overline{P}_{b'}^\beta} \sum_{l \in \mathcal{L}} \Delta p_{b',l,h}^{\beta,r,\uparrow/\downarrow} \quad \forall (b, b') \in \mathcal{B} \times \mathcal{B} \quad (29a)$$

$$\kappa_b^\beta \varsigma_{b,i,h}^{\beta,r,\uparrow/\downarrow} / \overline{P}_b^\beta = \kappa_i^g \Delta p_{i,h}^{g,r,\uparrow/\downarrow} / \overline{P}_i^g \quad \forall (b, i) \in \mathcal{B} \times \mathcal{I} \quad (29b)$$

$$\kappa_i^g \varsigma_{i',i,h}^{g,r,\uparrow/\downarrow} / \overline{P}_i^g = \kappa_{i'}^g \varsigma_{i',i,h}^{g,r,\uparrow/\downarrow} / \overline{P}_{i'}^g \quad \forall (i, i') \in \mathcal{I} \times \mathcal{I} \quad (29c)$$

$$\varsigma_{b,i,h}^{\beta,r,\uparrow/\downarrow} = u_{i,h} \sum_{l \in \mathcal{L}} \Delta p_{b,l,h}^{\beta,r,\uparrow/\downarrow}, \quad \varsigma_{i,i',h}^{g,r,\uparrow/\downarrow} = u_{i,h} \Delta p_{i',h}^{g,r,\uparrow/\downarrow} \quad (29d)$$

where  $\varsigma_{b,i,h}^{\beta,r,\uparrow/\downarrow}$  and  $\varsigma_{i',i,h}^{g,r,\uparrow/\downarrow}$  are auxiliary variables representing bilinear terms, so that the corresponding constraints can be linearized using standard integer optimization techniques [43].

Unlike the droop-only case, if a microgrid has a supplementary control like AGC, intra-dispatch fluctuations in the order of seconds are handled by such supplementary control and power sharing is no longer constrained. Thus, in this case constraints (29) are not needed.

#### D. Other Constraints

The remaining constraints for the proposed EMS model are presented here. Similar equations can already be found in the existing EMS literature [4]–[10]. The power balance is described as follows:

$$\sum_{b \in \mathcal{B}} \sum_{l \in \mathcal{L}} (d_{b,l,h} - c_{b,l,h}) + \sum_{i \in \mathcal{I}} \hat{p}_{i,h}^g = \hat{D}_h - n_h^w \hat{P}_h^w - n_h^s \hat{P}_h^s - l_{s_h} \quad \forall h \in \mathcal{H} \quad (30)$$

where the wind and solar average generation comes from (26); and  $l_{s_h}$  indicates average load shedding during dispatch time interval  $h$ .

The logic of commitment variables, and the minimum up/down constraints on thermal generators are described by the following equations:

$$u_{i,h} - u_{i,h-1} = v_{i,h} - w_{i,h} \quad (31a)$$

$$\sum_{m=h-M_i^{dn}}^{h-1} (1 - u_{i,m}) \Delta T_m \geq M_i^{dn} v_{i,h} \quad (31b)$$

$$\sum_{m=h-M_i^{up}}^{h-1} u_{i,m} \Delta T_m \geq M_i^{up} w_{i,h} \quad \forall i \in \mathcal{I}, h \in \mathcal{H} \quad (31c)$$

where  $v_{i,h}$  and  $w_{i,h}$  indicate the start-up/shut-down of generators; and,  $M_i^{up}$  and  $M_i^{dn}$  are the minimum up/down times.

Finally, an energy neutrality constraint is included to prevent significant deviations from the initial battery SoC:

$$s_{b,l,H} = S_{b,l}^0 \quad \forall b \in \mathcal{B}, l \in \mathcal{L} \quad (32)$$

where  $S_{b,l}^0$  is the initial battery SoC, and  $H$  is the last time index of the set of dispatch time intervals  $\mathcal{H} = \{1, \dots, H\}$ .

#### E. Optimization Model and Architecture

Based on the equations described in the previous sections, a novel EMS model with regulation, battery degradation, renewable curtailment, and power sharing limitations can be formulated. Thus, the EMS objective function  $\mathcal{F}(\cdot)$  is composed by a degradation component  $\Phi \in [0, 1]$ , variable generation costs  $C^g$ , no-load costs  $C^{nl}$ , start-up costs  $C^{su}$ , shut-down costs  $C^{sd}$ , and load shedding costs  $C^{ls}$ , as follows:

$$\begin{aligned} \mathcal{F}(\mathbf{x}, \mathbf{y}) = & \sum_{h \in \mathcal{H}} \sum_{b \in \mathcal{B}} \sum_{l \in \mathcal{L}} E_b \cdot RC_b \cdot \Phi_{b,l,h} + \sum_{h \in \mathcal{H}} C^{ls} \Delta T_h l_{s_h} \\ & + \sum_{h \in \mathcal{H}} \sum_{i \in \mathcal{I}} C_i^g \Delta T_h \left( \hat{p}_{i,h}^g + \Delta e_{i,h} \right) + \\ & \sum_{h \in \mathcal{H}} \sum_{i \in \mathcal{I}} \left( C_i^{nl} \Delta T_h u_{i,h} + C_i^{su} v_{i,h} + C_i^{sd} w_{i,h} \right) \end{aligned}$$

where  $E_b$  is battery's  $b$  energy capacity;  $RC_b$  is the replacement cost;  $\mathbf{x} = [\mathbf{u}, \mathbf{v}, \mathbf{w}]^T$  are the binary decision variables; and  $\mathbf{y} = [\hat{\mathbf{p}}^g, \Delta \mathbf{p}^g, \Delta \mathbf{p}^\beta, \mathbf{n}, \mathbf{s}, \mathbf{c}, \mathbf{d}, \mathbf{l}_s, \zeta, \varsigma]^T$  are the continuous decisions variables. This results in the following complete EMS model:

$$\min_{\mathbf{x}, \mathbf{y}} \mathcal{F}(\mathbf{x}, \mathbf{y}) \quad (33)$$

$$\text{s.t. } \mathbf{x} \in \{0, 1\}^n, \mathbf{y} \geq 0$$

Reserves and power balance: (11), (12), (28), (30)

Thermal generators: (17), (21), (31)

Batteries and degradation: (18), (19), (22)–(25), (32)

Renewable generation: (27)

Power sharing: (29) if droop-only control

which is a Mixed Integer Linear Programming (MILP) problem that can be solved by off-the-shelf solvers.

The general architecture of the proposed EMS is described in Fig. 3, which is based on a Model Predictive Control (MPC) scheme, as in [4]–[10]. Under this scheme, optimal dispatch set-points for the first dispatch time interval of each MPC iteration are regularly re-calculated and broadcasted to the microgrid's controllers based on frequently updated forecasts. Note that in the proposed EMS, participation factors  $\alpha$  are computed only if an AGC-like supplementary control is available, as these are not relevant in the case of droop-only control.

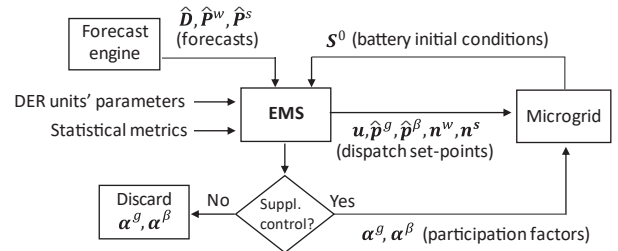


Fig. 3. Proposed EMS architecture

#### V. COMPUTATIONAL EXPERIMENTS

In this section, computational simulations to evaluate the performance of the proposed EMS model are presented. First,

the general settings of the simulations are presented in Section V-A. Then, the procedure used to calibrate reserve parameters are presented in Section V-B. Finally, specific settings, results and discussions, for each of the two evaluated test systems are presented in Sections V-C and V-D.

### A. General Settings

The performance of the proposed EMS is evaluated by simulating its implementation during one full day on the following 2 test systems [5]: a real isolated microgrid located in KLFN Ontario-Canada, and a larger test system based on a CIGRE medium voltage benchmark system. As in [4]–[10], simulations are performed considering a MPC scheme for which average power forecasts and optimal dispatch set-points are updated every 5 min, resulting in negligible average power forecast errors for the first dispatch time interval of each MPC iteration, i.e.,  $\chi_1^{mg}(\xi) \approx 0$ . In each MPC run, a 24h horizon is used, alongside a variable time-resolution with different time-steps  $\Delta T_h$ : 6 time-steps of 5min, 6 time-steps of 15min, 6 time-steps of 30min, and 19 time steps of 1h. To reduce computational burden, reserve requirements are only considered for the next 5 hours, i.e., first 18 dispatch time intervals.

In the simulations, it is assumed that set-points are determined by the EMS, and short-term fluctuations are managed either by a droop-only frequency control, or an AGC-like control with both droop and supplementary controls, as specified in each case. Also, it is assumed that forecast errors and their associated reserves are only defined for dispatch time intervals  $h \geq 2$ , as  $\chi_1^{mg}(\xi) \approx 0$  in accordance with the EMS's MPC scheme. Furthermore, it is assumed that all controllers are properly tuned, and thus degraded regulation performance can only arise from insufficient reserve allocation. In the event of reserve shortage, it is assumed that auxiliary emergency load shedding and renewable curtailment controllers are triggered, preventing system collapse.

For comparison purposes, three different EMS and frequency control architectures are evaluated in the simulations. The first one corresponds to the Base+Derating (B+DRT) architecture, in which a conventional EMS with a droop-only control is considered, similar to those proposed in [4]–[10]. In this architecture, uncertain power variations are assumed to be handled by: (i) a unique total reserve need, with no distinction between forecast errors or regulation, which is computed as a percentage of the forecast renewable generation and demand; and (ii) a power capacity derating of generators and batteries, which is computed as percentage of the unit's rating. Note that for this architecture, the change in the expected thermal average power (21) and SoC (22), battery degradation (25), the impact of renewable curtailment on reserve needs (28), and limitations on the sharing of intra-dispatch fluctuations (29) are not represented in the EMS.

The second and third architectures correspond to the Regulation+Droop (R+DRP) and Regulation+AGC (R+AGC) cases, where both consider the formulation described in Section IV-E for the EMS, and handle uncertain power variations through forecast error and regulation reserves, which are computed as a

percentage of the forecast renewable generation and demand. In both cases, 4 even partitions with  $\bar{s}_l = 0.2 \forall l \in \mathcal{L}$  are considered for the piecewise linear degradation model (4). A droop-only control is assumed in the R+DRP case, whereas an AGC-like control is assumed in the R+AGC case. Accordingly, power sharing constraints (29) are considered exclusively in the R+DRP case, and are enforced only for dispatch time intervals with a time-step equal to 5min, i.e., the first 6 dispatch time intervals.

The performance of the three architectures is evaluated by implementing the EMS's optimal dispatch decisions for the first dispatch time interval, and computing the corresponding reference  $\mathbf{p}$  and delivered  $\mathbf{p}'$  instantaneous powers (see Sections III-C and III-D). Delivered instantaneous powers are then used to compute the effective average thermal generation costs, battery degradation costs, load shedding, renewable curtailment, and total number of start-ups and shut-downs. Furthermore, security from a regulation perspective is measured by comparing reference and delivered powers and computing the resulting LHP (16), which indicates the percentage of time that insufficient reserves were allocated.

Reserve sizing parameters were computed based on [10] and [39]. Specifically, standard deviations of forecast errors  $\tilde{\sigma}_h^x$  were quantified by linear interpolations using the 1h-ahead and 24h-ahead values reported in [10] (see Table I), whereas standard deviations of intra-dispatch fluctuations  $\tilde{\sigma}_h^r$  were calculated using 6-weeks measurements from KLFN microgrid with a resolution of  $\Delta\tau = 1s$  (see Table II) [39]. Battery degradation parameters are taken from [37], and the effective degradation resulting from the simulations is obtained using the detailed degradation model (3), which is then multiplied by the battery's replacement costs to obtain the resulting degradation costs. The reduction of the battery's energy capacity due to cell capacity fading is not considered in the simulations, as such reduction is negligible within the simulated daily horizon [37]. All simulations are performed using the Julia programming language, JuMP package, and Gurobi solver, on a PC with an Intel Core i7 3.20-GHz processor and 16 GB of RAM under a 64-bit Windows 10 operating system.

### B. Tuning of Reserve Parameters

To ensure a fair comparison between B+DRT, R+DRP, and R+AGC, reserve needs and capacity deratings are calibrated in each case study, so that the resulting load shedding and LHP obtained in the simulations are the same for the three architectures. In the case of load shedding, total reserve needs for B+DRT, and forecast error reserve needs for R+DRP and R+AGC, are determined such that a zero load shedding is obtained in all the case studies. For both KLFN and CIGRE test systems, this is achieved by considering one standard deviation of the forecast errors (see Table I) when computing the reserve needs as a percentage of the forecast renewable generation and load.

In the case of LHP, reserve quantification required a more delicate tuning to ensure that, for each case study, the same LHP is obtained in the three architectures. On the one hand, for B+DRT, simulations showed that directly increasing the

TABLE I  
STANDARD DEVIATION OF FORECAST ERRORS [10]

Source	1h-ahead [%]	24h-ahead [%]
Wind	14.70	30.92
Solar	10.20	14.02
Demand	11.62	15.78

TABLE II  
STANDARD DEVIATION OF INTRA-DISPATCH FLUCTUATIONS [39]

Source	5min [%]	15min [%]	30min [%]	1h [%]
Wind	35.43	39.90	42.35	44.58
Solar	16.69	24.54	27.91	33.21
Demand	3.68	6.27	8.93	12.63

total reserve needs did not reduce the LHP, since the basic EMS neglected the effect of droops and typically dispatched generators at maximum power and left the provision of reserves to the batteries, leaving no room in generators for handling intra-dispatch fluctuations. This in turn meant that the generators' maximum capacity limit was repeatedly reached, since for a droop-only control a percentage of the intra-dispatch fluctuations are forcedly allocated to generators based on their droop gains. Thus, for B+DRT, LHP was calibrated by applying a power capacity percentage derating to generators and batteries. Specifically, the maximum (minimum) capacity limits of generators and batteries considered in the basic EMS were reduced (increased) using a percentage of their installed capacity. This way, some room for handling intra-dispatch fluctuations is always left when determining the average power set-points in the basic EMS. On the other hand, for R+DRP and R+AGC, LHP was directly adjusted by increasing the regulation reserves through the parameter  $\epsilon_r$ , greatly simplifying the tuning process due to the explicit modeling of intra-dispatch fluctuations.

### C. KLFN Microgrid: Settings, Results and Discussion

The performance of the proposed EMS is first evaluated on a test system based on the real-world isolated KLFN microgrid, for which real generation and demand measurements are used [39]. This microgrid is composed of 3 diesel units with capacities of 1500kW, 1000kW, and 600kW, which are only operated one at a time, as per the utility's dispatch rules, and whose parameters are extracted from [5]. For the simulated day, the 600kW unit is assumed to be ON at the start of the day, and a 1026kW peak demand is reached during the evening.

Currently, the KLFN microgrid has low renewable penetration (less than 70kW installed capacity) and no energy storage system; thus, regulation and battery degradation are not an issue at the present time. Therefore, to better illustrate the features of the proposed EMS for regulation and battery degradation modeling, a 1000kW/1000kWh lithium-ion battery is considered, and the renewable installed capacity is increased to reach a 25% renewable energy share (12.5% wind and 12.5% solar) in the simulated day. Additional details about the test system are presented in the Appendix.

The simulation results for KLFN microgrid are shown in Table III, for which three different regulation security levels

are defined based on the resulting LHP: low (10%), medium (5%) and high (1%). Observe that only a small capacity derating ( $\leq 6\%$ ) is needed to reach the desired regulation security levels for the basic EMS (B+DRT), as the KLFN test system has a medium renewable energy share (25%), and its generators and battery have a relatively large power capacity compared to the system's peak load.

The benefits of implementing the proposed EMS model in the KLFN microgrid can be observed in the total costs, degradation costs, and number of and start-ups (shut-downs) reported in Table III. Note that the proposed EMS (R+DRP and R+AGC) outperforms the basic EMS (B+DRT) for all regulation security levels in terms of total costs (1%-9% daily savings), battery degradation (86%-93% reduction), and thermal unit cycling (less start-ups and shut-downs), while keeping computational tractability (less than 1 s per MPC iteration). Moreover, observe how the proposed EMS uses renewable curtailment to reduce reserve needs and thus obtain better solutions; and that for small microgrids, such as KLFN, the difference between having a simple droop-only control (R+DRP) and a more advanced AGC (R+AGC) is insignificant in terms of operating costs.

### D. CIGRE Microgrid: Settings, Results and Discussion

The proposed EMS is evaluated here on a more complex microgrid based on a modified CIGRE benchmark test system from [5]. This microgrid has a 5755 kW peak demand, and is composed of 3 diesel generators (4700kW combined capacity) and 2 Combined Heat-and-Power units (810kW combined capacity). The microgrid also has multiple energy storage systems, with a total installed capacity of 1324kW/1324kWh, which for simplicity are modeled as a single lithium-ion battery. Also, the renewable installed capacity is increased to reach a 50% renewable energy share. Additional details about the test system are presented in the Appendix.

The simulation results for the CIGRE microgrid are shown in Table IV. Unlike the KLFN microgrid, a significant derating ( $\geq 19\%$ ) and load shedding is needed for the basic EMS (B+DRT) to reach the desired LHP, which in turn causes a pronounced increase in total costs for the medium and high regulation security levels. Furthermore, note that the basic EMS is only able to reach a minimum of 2.3% (instead of 1%) LHP for the high regulation security level. This poor performance results from the large renewable energy share (50%) of the test system, alongside the inadequacy of the basic EMS to properly model large intra-dispatch power fluctuations. In contrast, the proposed EMSs (R+DRT and R+AGC) yield the desired LHP at reduced costs, since short-term fluctuations are properly modeled in this case.

As also noted for the KLFN microgrid, the proposed EMSs show overall better performance for the CIGRE system in terms of battery degradation and thermal unit cycling, while keeping computational tractability, and also use renewable curtailment as a reserve management mechanism. However, and unlike the small KLFN microgrid, the use of an AGC (R+AGC) instead of a simple droop-only control (R+DRP) may yield significant savings in terms of operating costs for the more complex CIGRE microgrid (3%-18% cost reduction).

In summary, the proposed EMS model outperforms the conventional EMS model, achieving reduced operational costs, battery degradation, and thermal unit cycling in both test systems for a wide range of regulation security levels, while maintaining computational tractability. This overall better performance is the result of explicitly modeling intra-dispatch fluctuations and their impact on reserve needs, battery degradation, and renewable curtailment.

## VI. CONCLUSIONS

Second-to-second power imbalances stemming from renewable generation can severely hinder the regulation performance of sustainable isolated microgrids, as these are typically characterized by a high renewable energy penetration and low inertia. Motivated by this, the present paper develops a computationally efficient and practically implementable EMS that models the operational impact of intra-dispatch fluctuations and battery degradation. The proposed EMS was evaluated on two realistic test systems, showing the benefits of including intra-dispatch fluctuations and battery degradation in the decision-making process of the EMS. Such benefits include, among others, the reduction of the microgrid's total operating costs, battery degradation, and thermal unit cycling.

The results presented in this paper substantiate the need to incorporate the impact of fast power dynamics and primary frequency controllers in microgrid operational models. Future work will focus on developing computationally efficient models that describe the impact of short-term power imbalances on frequency dynamics, so that a computationally tractable frequency-constrained EMS can be designed.

## APPENDIX

Additional test system parameters are presented in this appendix. For both the KLFN and CIGRE test systems, Li(NiMnCo)O<sub>2</sub>-based batteries are considered, which have the following cycle depth stress function:

$$\Gamma_{\theta}(\theta) = (5.23 \times 10^{-3}) \theta^{2.03}$$

with battery replacement cost of 300 USD/kWh [37]. Furthermore, the considered batteries have an initial SoC of 50%, and corresponding limits of 10% and 90%. For the KLFN test system, a charging and discharging efficiency of  $\eta_b^c = \eta_b^d = 95\%$  is used [37]; on the other hand, for the CIGRE test system, an efficiency of  $\eta_b^c = \eta_b^d = 86\%$  is used [5].

Generator parameters for the KLFN and CIGRE test systems are presented in Tables V and VI, respectively. These parameters are based on [5], with the only difference that the fuel costs have been linearized to speed-up simulations; note that this linearized version is highly accurate, having a coefficient of determination greater than 95%. A load shedding cost of 12 USD/kWh, as per [44], and droop  $\kappa = 3\%$  for all units, as per [40], are used in all simulations.

## REFERENCES

- [1] D. E. Olivares *et al.*, "Trends in microgrid control," *IEEE Trans. Smart Grid*, vol. 5, no. 4, pp. 1905–1919, 2014.
- [2] M. F. Zia, E. Elbouchikhi, and M. Benbouzid, "Microgrids energy management systems: A critical review on methods, solutions, and prospects," *Applied Energy*, vol. 222, pp. 1033 – 1055, 2018.
- [3] H. Shayeghi, E. Shahryari, M. Moradzadeh, and P. Siano, "A survey on microgrid energy management considering flexible energy sources," *Energies*, vol. 12, no. 11, 2019.
- [4] D. E. Olivares, C. A. Cañizares, and M. Kazerani, "A centralized energy management system for isolated microgrids," *IEEE Trans. Smart Grid*, vol. 5, no. 4, pp. 1864–1875, 2014.
- [5] B. V. Solanki, C. A. Cañizares, and K. Bhattacharya, "Practical energy management systems for isolated microgrids," *IEEE Trans. Smart Grid*, vol. 10, no. 5, pp. 4762–4775, 2019.
- [6] M. Farrokhhabadi, C. A. Cañizares, and K. Bhattacharya, "Unit commitment for isolated microgrids considering frequency control," *IEEE Trans. Smart Grid*, vol. 9, no. 4, pp. 3270–3280, 2018.
- [7] B. V. Solanki, A. Raghurajan, K. Bhattacharya, and C. A. Cañizares, "Including smart loads for optimal demand response in integrated energy management systems for isolated microgrids," *IEEE Trans. Smart Grid*, vol. 8, no. 4, pp. 1739–1748, 2017.
- [8] P. S. Sauter *et al.*, "Electric thermal storage system impact on northern communities' microgrids," *IEEE Transactions on Smart Grid*, vol. 10, no. 1, pp. 852–863, 2019.
- [9] W. Violante, C. A. Cañizares, M. A. Trovato, and G. Forte, "An energy management system for isolated microgrids with thermal energy resources," *IEEE Transactions on Smart Grid*, vol. 11, no. 4, pp. 2880–2891, 2020.
- [10] R. Palma-Behnke *et al.*, "A microgrid energy management system based on the rolling horizon strategy," *IEEE Trans. Smart Grid*, vol. 4, no. 2, pp. 996–1006, 2013.
- [11] M. A. Nasr *et al.*, "A multi-objective voltage stability constrained energy management system for isolated microgrids," *International Journal of Electrical Power & Energy Systems*, vol. 117, p. 105646, 2020.
- [12] M. F. Zia, E. Elbouchikhi, M. Benbouzid, and J. M. Guerrero, "Energy management system for an islanded microgrid with convex relaxation," *IEEE Transactions on Industry Applications*, vol. 55, no. 6, pp. 7175–7185, 2019.
- [13] M. Manbachi and M. Ordóñez, "AMI-based energy management for islanded ac/dc microgrids utilizing energy conservation and optimization," *IEEE Transactions on Smart Grid*, vol. 10, no. 1, pp. 293–304, 2019.
- [14] M. Farrokhhabadi *et al.*, "Microgrid stability definitions, analysis, and examples," *IEEE Trans. Power Syst.*, vol. 35, no. 1, pp. 13–29, 2020.
- [15] P. Zeng, H. Li, H. He, and S. Li, "Dynamic energy management of a microgrid using approximate dynamic programming and deep recurrent neural network learning," *IEEE Transactions on Smart Grid*, vol. 10, no. 4, pp. 4435–4445, 2019.
- [16] H. Çimen, N. Çetinkaya, J. C. Vasquez, and J. M. Guerrero, "A microgrid energy management system based on non-intrusive load monitoring via multitask learning," *IEEE Transactions on Smart Grid*, vol. 12, no. 2, pp. 977–987, 2021.
- [17] Q. Sui *et al.*, "Day-ahead energy management for pelagic island microgrid groups considering non-integer-hour energy transmission," *IEEE Transactions on Smart Grid*, vol. 11, no. 6, pp. 5249–5259, 2020.
- [18] C. Wang *et al.*, "Optimal management for grid-connected three/single-phase hybrid multimicrogrids," *IEEE Transactions on Sustainable Energy*, vol. 11, no. 3, pp. 1870–1882, 2020.
- [19] M. Anvari *et al.*, "Short term fluctuations of wind and solar power systems," *New Journal of Physics*, vol. 18, no. 6, 2016.
- [20] H. Bevrani, A. Ghosh, and G. Ledwich, "Renewable energy sources and frequency regulation: survey and new perspectives," *IET Renewable Power Generation*, vol. 4, no. 5, pp. 438–457, 2010.
- [21] H. Banakar, C. Luo, and B. T. Ooi, "Impacts of wind power minute-to-minute variations on power system operation," *IEEE Transactions on Power Systems*, vol. 23, no. 1, pp. 150–160, 2008.
- [22] E. Ela and M. O'Malley, "Studying the variability and uncertainty impacts of variable generation at multiple timescales," *IEEE Transactions on Power Systems*, vol. 27, no. 3, pp. 1324–1333, 2012.
- [23] M. H. Athari and Z. Wang, "Impacts of wind power uncertainty on grid vulnerability to cascading overload failures," *IEEE Transactions on Sustainable Energy*, vol. 9, no. 1, pp. 128–137, 2018.
- [24] L. Che, X. Liu, and Z. Li, "An intrainterval security risk regarding regulation burden due to wind variation in high-wind-penetrated power systems," *IEEE Transactions on Power Systems*, vol. 33, no. 3, pp. 3213–3216, 2018.

TABLE III  
COMPARISON FOR KLFN SYSTEM WITH 25% RENEWABLE ENERGY SHARE

Regul. Secur.	EMS Model	Derating [%] or $\epsilon_r$	LHP [%]	Total Costs [USD]	Thermal Costs [USD]	Degrad. Costs [USD]	Load Shed. [kWh]	Renew. Curt. [kWh]	Start-ups (Shut-downs)	Comp. Time [s]
Low	B+DRT	2.0%	9.9	3081.6	2886.8	194.8	0.0	0.0	6 (7)	0.3
	R+DRP	0.215	9.6	2809.8	2782.8	27.0	0.0	118.2	1 (1)	0.7
	R+AGC	0.220	9.7	2813.3	2800.8	12.5	0.0	118.2	0 (0)	0.6
Medium	B+DRT	3.0%	5.0	2906.2	2692.3	213.9	0.0	0.0	3 (4)	0.3
	R+DRP	0.500	5.1	2809.9	2794.2	15.7	0.0	118.2	0 (0)	0.7
	R+AGC	0.600	4.9	2808.8	2794.4	14.4	0.0	118.2	0 (0)	0.6
High	B+DRT	6.0%	0.9	2846.4	2679.6	166.8	0.0	0.0	4 (4)	0.3
	R+DRP	1.500	1.0	2810.8	2793.9	16.9	0.0	118.2	0 (0)	0.7
	R+AGC	1.300	1.1	2796.4	2785.4	11.0	0.0	118.2	0 (0)	0.6

TABLE IV  
COMPARISON FOR CIGRE SYSTEM WITH 50% RENEWABLE ENERGY SHARE

Regul. Secur.	EMS Model	Derating [%] or $\epsilon_r$	LHP [%]	Total Costs [USD]	Thermal Costs [USD]	Degrad. Costs [USD]	Load Shed. [kWh]	Renew. Curt. [kWh]	Start-ups (Shut-downs)	Comp. Time [s]
Low	B+DRT	19.0%	10.2	8596.6	8436.6	160.0	0.0	78.7	19 (17)	0.5
	R+DRP	1.130	10.1	8732.2	8596.1	136.0	0.0	2263.3	17 (15)	3.6
	R+AGC	1.000	10.4	8481.1	8423.4	57.7	0.0	1643.8	12 (10)	2.5
Medium	B+DRT	28.5%	4.8	11583.6	8917.1	249.1	201.4	416.2	22 (20)	0.5
	R+DRP	1.500	5.1	9151.4	8983.4	168.1	0.0	4211.3	12 (10)	4.8
	R+AGC	1.300	4.9	8433.7	8359.5	74.2	0.0	2094.6	12 (10)	2.8
High	B+DRT	30.0%	2.3 <sup>†</sup>	60888.1	8761.7	331.5	4316.2	3300.6	20 (17)	0.2
	R+DRP	3.000	0.8	10665.5	10533.7	131.8	0.0	10401.7	12 (9)	7.5
	R+AGC	2.500	0.9	8705.4	8633.9	71.5	0.0	3622.2	12 (10)	3.0

<sup>†</sup>1% LHP could not be achieved. Instead, the minimum achievable LHP is indicated

TABLE V  
GENERATOR PARAMETERS FOR KLFN TEST SYSTEM

Unit	$\bar{P}_i^g$ [kW]	$P_i^g$ [kW]	$C_i^g$ [USD/kW-min]	$C_i^{nl}$ [USD/min]	$C_i^{su}$ [USD]	$C_i^{sd}$ [USD]	$M_i^{up}$ [min]	$M_i^{dn}$ [min]
1	1500	600	0.021017	-0.3184	83.60	13.464	30	30
2	1000	400	0.008333	1.4678	36.90	7.304	30	30
3	600	180	0.003088	0.5891	13.20	4.664	30	30

TABLE VI  
GENERATOR PARAMETERS FOR CIGRE BENCHMARK TEST SYSTEM

Unit	$\bar{P}_i^g$ [kW]	$P_i^g$ [kW]	$C_i^g$ [USD/kW-min]	$C_i^{nl}$ [USD/min]	$C_i^{su}$ [USD]	$C_i^{sd}$ [USD]	$M_i^{up}$ [min]	$M_i^{dn}$ [min]
1	2500	1000	0.003797	0.2493	83.60	13.464	60	60
2	1400	600	0.003767	0.3740	39.60	7.304	60	60
3	800	350	0.004217	0.1100	13.20	4.664	30	30
4	310	60	0.004217	0	6.47	1.267	30	30
5	500	100	0.001067	-0.1067	0.83	0	30	30

- [25] L. Che *et al.*, "Intra-interval security assessment in power systems with high wind penetration," *IEEE Transactions on Sustainable Energy*, vol. 10, no. 4, pp. 1890–1903, 2019.
- [26] Y. Zhang *et al.*, "Impact analysis of intra-interval variation on dynamic security assessment of wind-energy power systems," in *2020 IEEE Power Energy Society General Meeting (PESGM)*, 2020, pp. 1–5.
- [27] Z. Bao *et al.*, "A multi time-scale and multi energy-type coordinated microgrid scheduling solution—part i: Model and methodology," *IEEE Transactions on Power Systems*, vol. 30, no. 5, pp. 2257–2266, 2015.
- [28] C. Ju, P. Wang, L. Goel, and Y. Xu, "A two-layer energy management system for microgrids with hybrid energy storage considering degradation costs," *IEEE Trans. Smart Grid*, vol. 9, no. 6, pp. 6047–6057, 2018.
- [29] C. Zhang, Y. Xu, Z. Y. Dong, and J. Ma, "Robust operation of microgrids via two-stage coordinated energy storage and direct load control," *IEEE Trans. Power Syst.*, vol. 32, no. 4, pp. 2858–2868, 2017.
- [30] M. I. Alizadeh, M. P. Moghaddam, and N. Amjadi, "Multistage multiresolution robust unit commitment with nondeterministic flexible ramp considering load and wind variabilities," *IEEE Transactions on Sustainable Energy*, vol. 9, no. 2, 2018.
- [31] L. Che *et al.*, "Intra-interval security based dispatch for power systems with high wind penetration," *IEEE Transactions on Power Systems*, vol. 34, no. 2, pp. 1243–1255, 2019.
- [32] X. Hu, C. Zou, C. Zhang, and Y. Li, "Technological developments in batteries: A survey of principal roles, types, and management needs," *IEEE Power and Energy Magazine*, vol. 15, no. 5, pp. 20–31, 2017.
- [33] L. Bird, J. Cochran, and X. Wang, "Wind and solar energy curtailment: Experience and practices in the united states," National Renewable Energy Lab, Tech. Rep., 2014.
- [34] B. Xu *et al.*, "Modeling of lithium-ion battery degradation for cell life assessment," *IEEE Trans. Smart Grid*, vol. 9, no. 2, pp. 1131–1140, 2018.
- [35] T. A. Nguyen and M. L. Crow, "Stochastic optimization of renewable-based microgrid operation incorporating battery operating cost," *IEEE Trans. Power Syst.*, vol. 31, no. 3, pp. 2289–2296, 2016.
- [36] I. Duggal and B. Venkatesh, "Short-term scheduling of thermal generators and battery storage with depth of discharge-based cost model," *IEEE Trans. Power Syst.*, vol. 30, no. 4, pp. 2110–2118, 2015.
- [37] B. Xu *et al.*, "Factoring the cycle aging cost of batteries participating in electricity markets," *IEEE Trans. Power Syst.*, vol. 33, no. 2, pp. 2248–2259, 2018.
- [38] B. Xu, Y. Shi, D. S. Kirschen, and B. Zhang, "Optimal battery participation in frequency regulation markets," *IEEE Trans. Power Syst.*, vol. 33, no. 6, pp. 6715–6725, 2018.
- [39] M. Arriaga and C. Cañizares, "Overview and Analysis of Data for Microgrid at Kasabonika Lake First Nation (KLFN)," Hatch Project,

University of Waterloo, Tech. Rep., 2015.

- [40] A. Wood, B. Wollenberg, and G. Sheblé, *Power Generation, Operation, and Control*, 3rd ed. Wiley, 2013, ch. 10, pp. 468–500.
- [41] R. C. Geary, “Moments of the ratio of the mean deviation to the standard deviation for normal samples,” *Biometrika*, vol. 28, no. 3, pp. 295–307, 1936.
- [42] S. Boyd and L. Vandenberghe, “Localization and cutting-plane methods,” Stanford EE 364b course, Lecture notes, 2007.
- [43] A. Gupte, S. Ahmed, M. S. Cheon, and S. Dey, “Solving mixed integer bilinear problems using MILP formulations,” *SIAM Journal on Optimization*, vol. 23, no. 2, pp. 721–744, 2013.
- [44] A. J. Praktijnko, A. Hähnel, and G. Erdmann, “Assessing energy supply security: Outage costs in private households,” *Energy Policy*, vol. 39, no. 12, pp. 7825 – 7833, 2011.



**Samuel Córdova** (S'18) received the M.Sc. degree in electrical engineering from the Pontificia Universidad Católica de Chile (Santiago, Chile) and is currently working towards a Ph.D. degree in electrical engineering at both the University of Waterloo (Waterloo, ON, Canada) and Pontificia Universidad Católica de Chile under a cotutelle agreement. He has worked as a R&D Engineer at the Systep Ingeniería and Vinken consulting firms in Chile and performed various studies for the Chilean system operator. His main research interest include

the operation and control of modern power systems with significant renewable integration in the context of smart grids.



**Claudio Cañizares** (S'85-M'91-SM'00-F'07) is a University Professor, the Hydro One Endowed Chair, and the Executive Director of the Waterloo Institute for Sustainable Energy (WISE) at the ECE Department of the University of Waterloo, where he has been since 1993. His highly cited research focuses on modeling, simulation, computation, stability, control, and optimization of power and energy systems. He is the IEEE Trans. Smart Grid EIC; Division VII Director-Elect to the IEEE Board; a Fellow of the IEEE, the Royal Society of Canada, and the

Canadian Academy of Engineering; and has received the 2017 IEEE PES Outstanding Power Engineering Educator Award, the 2016 IEEE Canada Electric Power Medal, and multiple awards and recognitions from PES Technical Committees.



**Álvaro Lorca** (M'17) is an Assistant Professor in the Department of Electrical Engineering and the Department of Industrial and Systems Engineering at Pontificia Universidad Católica de Chile. He is also co-director of Vinken, a business unit at Dictuc dedicated to specialized consulting, advanced research, and technological developments for the energy industry. He received a Ph.D. in Operations Research from Georgia Institute of Technology, and an M.Sc. in Engineering and an Industrial Engineering degree with a diploma in Mathematical Engineering from

Pontificia Universidad Católica de Chile. His research and professional activities are centered in the application of mathematical methods and data science in energy planning, power system operations, renewable energy integration, smart grids, and resilience, among other topics. He has published in various specialized scientific journals, including *Operations Research*, *European Journal of Operational Research*, *Production and Operations Management*, *IEEE Transactions on Power Systems*, *Energy*, *Energy Economics*, *Applied Energy*, and *Energy Policy*, among others. He has worked with ISO New England, World Bank, Environmental Defense Fund, Coordinador Eléctrico Nacional, Comisión Nacional de Energía, Chilean Ministry of Energy, Transelec, and Fraunhofer Chile Research, among others. His research has been recognized with various awards, including the Best Paper in Energy Award from the INFORMS Section on Energy, Natural Resources, and the Environment, and the Best Paper Award from the IEEE Power and Energy Society.



**Daniel E. Olivares** (S'11-M'14) was born in Santiago, Chile. He received the B.Sc. and Engineering degrees in electrical engineering from the University of Chile, Santiago, in 2006 and 2008, respectively, and the Ph.D. degree in electrical and computer engineering from the University of Waterloo, Waterloo, ON, Canada, in 2014. He is currently an Associate Professor in the Faculty of Engineering and Sciences at Adolfo Ibañez University, Chile. His research interests include modeling, simulation, and control, and optimization of power systems in the

context of smart grids.